

Article

The Stability of Dams with Different Stopping Elevations in the Tongling Valley-Type Tailings Impoundment: A Case Study in Yunnan China

Yiwen Pan ^{1,2}, Jianping Chen ^{1,2,*}, Xiaohuan Zuo ³, Cheng Zhang ^{1,2} and Shuangshuang Wu ^{1,2}

¹ School of Earth Sciences and Resources, China University of Geosciences, Beijing 100083, China; panyw@email.cugb.edu.cn (Y.P.); 3001210074@email.cugb.edu.cn (C.Z.); wss0805@163.com (S.W.)

² Beijing Key Laboratory of Development and Research for Land Resources Information, Beijing 100083, China

³ School of Emergency Management and Safety Engineering, China University of Mining and Technology Beijing 100083, China; zxh180329@163.com

* Correspondence: 3s@cugb.edu.cn

Abstract: Significant interest has been focused on recovery rates, recovery options, and recovery utilization when tailings impoundments are re-mined. However, the stability of the tailings dams during the recovery process is also a severe issue. Based on engineering geological surveys and laboratory tests, the evolution of the Tongling tailings impoundment's instability characteristics under different recovery heights and diverse working conditions was analyzed by numerical simulation. Firstly, with the help of 2D software, the position of the tailings dam infiltration line and the alteration of the dam safety factor during the stopping process were calculated. Secondly, 3Dmine (2017) software was used to create the 3D surface structure of the tailings impoundment, and then a 3D numerical analysis model was established by means of Midas GTS NX software. The numerical simulation of seepage and stress analyses were conducted based on the model. Consequently, the evolution of the stability characteristics of tailings dam under different operating conditions was calculated. The research demonstrates that the dry beach length of the tailings pond gradually reduces with a decrease in the extraction height, resulting in a lower infiltration line. Under flood conditions, the saturation line has partial overflow due to the poor seepage discharge capacity of the dam. The total displacement of the dam body is inversely proportional to the retrieval height. The more extreme the analyzed working conditions, the more the safety factor will be reduced. Additionally, the plastic variation area of the dam body will be more comprehensive, which will increase the risk of a dam collapse.

Keywords: tailings impoundment stopping; dam stability; displacement field; stress fields; different working conditions; numerical simulation



Citation: Pan, Y.; Chen, J.; Zuo, X.; Zhang, C.; Wu, S. The Stability of Dams with Different Stopping Elevations in the Tongling Valley-Type Tailings Impoundment: A Case Study in Yunnan China.

Minerals **2023**, *13*, 1365. <https://doi.org/10.3390/min13111365>

Academic Editors: Kun Du, Jianping Sun and Mamadou Fall

Received: 31 August 2023

Revised: 11 October 2023

Accepted: 24 October 2023

Published: 26 October 2023



Copyright: © 2023 by the authors. Licensee MDPI, Basel, Switzerland. This article is an open access article distributed under the terms and conditions of the Creative Commons Attribution (CC BY) license (<https://creativecommons.org/licenses/by/4.0/>).

1. Introduction

Tailings impoundments are usually used to accumulate various types of mineral wastes generated in the process of mining and beneficiation, and are essential facilities for mine safety production [1–4]. The treatment and management of tailings present significant global environmental and economic challenges. Inadequate management of tailings impoundments can result in severe environmental pollution and disasters [5]. In Europe, research primarily focuses on tailings impoundment management and pollution control [6]. Researchers are actively working on innovative techniques, including mechanochemical activation methods, to enhance resource recovery rates and reduce waste production [7]. Additionally, various safety monitoring measures have been implemented to prevent pollution from tailings impoundments, particularly heavy metal contamination [8]. In the Americas, research is centered on assessing the environmental impacts of tailings impoundments. For instance, studies have revealed that tailings impoundment leakage can have

profound effects on downstream lake systems [9,10]. The research direction in Africa is significantly different from that in Europe and the United States. Africa is rich in diamond, platinum group, and other metal resources, which produce a large amount of such metals every year, providing opportunities for carbon remediation methods such as alkalinity production and mineral carbonation. How to reduce the impact of tailings on the environment and human beings is an important research topic in Africa [11,12].

Tailings impoundments pose potential hazards. Yin et al. summarized the characteristics of tailings ponds in China, which are numerous in number, multifarious in types, and occupy an extensive land area [5]. Edraki et al. reported that numerous tailings dams have collapsed over the years, bringing catastrophic damage to the economy, residents' lives, and ecosystems downstream of the tailings impoundments [6]. A tailings impoundment failure would not only destroy mine infrastructure, but the spilled tailings would also lead to serious damage to the surrounding ecological environment [7–10]. Secondary disasters such as landslides, floods, and debris flows will occur if a tailings dam fails [11–13]. Luino et al. presented that in 1985, a tailings pond collapsed near Stava in northern Italy, killing 286 people [14]. On 8 September 2008, a particularly serious tailings dam burst occurred in Shanxi, China, resulting in 281 deaths and significant economic losses to the residents of the mine and downstream [15], which was reported by Gomes et al. In November 2015, the Fundão tailings pond in Brazil collapsed, releasing over 50 million cubic meters of tailings. Villages downstream were washed away, and the surrounding ecosystem was destroyed. Agurto Detzel et al. informed that in November of the same year, the Samarco tailings pond in Brazil was destabilized, leaking over 30 million cubic meters of tailings [16]. On 25 January 2019, the tailings pond failed catastrophically in Brumadinho, Brazil, killing 363 people and causing serious environmental pollution [17], which was reported by Silva Rotta et al.

A large quantity of existing tailings impoundments is out of use in China, which have outstanding potential problems. The basic flood discharge facilities of the abandoned tailings impoundments cannot be checked and maintained in time, which will lead to the tailings impoundments becoming dangerous reservoirs and increasing the risk of a tailings dam breach. Meanwhile, the tailings contain a variety of complex heavy metal ions, and the heavy metal pollution of tailings is a severe environmental problem [18–20]. Tailings contain a variety of helpful components that can be recycled [21–23]. If tailings impoundments can be reasonably remined, it not only enables the rational recycling of resources but also dramatically reduces or even eliminates the risk of tailings pond collapse and reduces the tailings pond failure rate [24–27]. Furthermore, reclaiming abandoned tailings impoundments brings certain economic benefits to mines and protects the ecological environment [28–30]. Tailings generally have high water content and high compressibility [31,32]. It is a significant potential threat to mine safety and production [33], which was proposed by Wei et al. Unlike ordinary reservoirs, tailings impoundments contain various chemical substances produced in the mineral processing process [34,35]. Moreover, the diameter of the tailings is small, the mechanical properties are poor, and the shear strength is low [36–38]. In the process of the continuous accumulation of tailings, tailing materials will produce chemical siltation, biological siltation, and physical siltation, resulting in a reduction in the consolidation and drainage capacity of tailings ponds, which will make them more susceptible to dam failure [39–41]. Additionally, Zhang et al. summarized that as the tailings dam body is raised, the risk of dam failure increases [42]. External factors such as heavy rainfall, flooding, and earthquakes can also exacerbate tailings impoundment accidents during the operation of tailings impoundments. Previous studies have found that tailings dam reservoir levels, tailings reservoir drainage systems, foundation stability, seepage effects, seismic liquefaction, the depth of the infiltration line, the flooding of the dam, and the length of the dam's dry bank are the most critical factors directly affecting the safe operation of tailings ponds [43–45]. Therefore, based on the above research results, it is of great theoretical significance and practical value to carry out seepage analyses, flooding

analyses, and seismic analyses for the safe operation of tailings dams. Designing reasonable mining plans for the tailings ponds is also necessary.

There are few studies on the stability analysis of the dam body during tailing reservoir mining. However, tailing pond mining is a dynamic process. In the process of mining, the dam will reduce the load slowly, and the height of the dam body will decrease gradually. The combined effect of these can cause changes in the dry beach length and the buried depth of the infiltration line, which will affect the stability of the dam. Since the Tongling tailings impoundment is adjacent to an open-pit stope, the dam's stability is directly related to the safety production of the whole mine. The Tongling tailings impoundment is a valley-type tailings impoundment. In a valley-type tailings impoundment, two-dimensional analysis cannot fully evaluate the displacement field and stress field variation characteristics in the three directions of the tailings dam. The main purpose of this research is to analyze the stability characteristics of the Tongling tailings impoundment under different recovery heights and diverse working conditions. The instability characteristics of the dam body are calculated under different working conditions (such as strong rainfall, floods, and earthquakes) by a combination of 2D and 3D numerical simulation analysis. As a result, the Tongling tailings impoundment retreatment plan has not yet been implemented in the actual engineering. It is essential to design a reasonable mining plan for the tailing pond. This analysis makes it possible to identify the main factors affecting the stability of the dam in advance, and it is helpful in taking the appropriate protective measures in later engineering practice. The stopping of the tailings impoundment is of great significance to the ecological environment and the safe production of mines. Moreover, the research can provide a corresponding reference for later engineering practice.

2. Materials and Methods

2.1. Study Area

This research paper focuses on valley-type tailings impoundments. Valley-type tailings impoundments are a preferred safe storage method for tailings, mainly established in regions with rugged natural landscapes or numerous mountains, such as South America, North America, Asia, and some areas of Africa. Based on a comprehensive analysis of similar tailings impoundments around the world, we found that most of the disasters caused by this type of tailings dam are due to intense precipitation and earthquake events. Typically, valley-type tailings impoundments are located in low-lying areas at the mouth of a valley, resulting in a relatively large catchment area but with limited flood regulation capacity. Therefore, in the regions we have studied, the primary considerations for the stability of tailings impoundments are various extreme conditions, such as intense precipitation, floods, and earthquakes.

The Tongling tailings impoundment has been out of service for many years (Figure 1). An open-pit mine has been opened near the tailings pond, which is located within the open pit boundary (Figure 2). In order to ensure the safety of the open pit, the Tongling tailings pond now needs to be written off and progressively re-mined. After recovery, the tailings will be transferred to another tailings pond in the mine. After the mining is completed, all tailings facilities will be dismantled, eventually restoring the original gully landform.

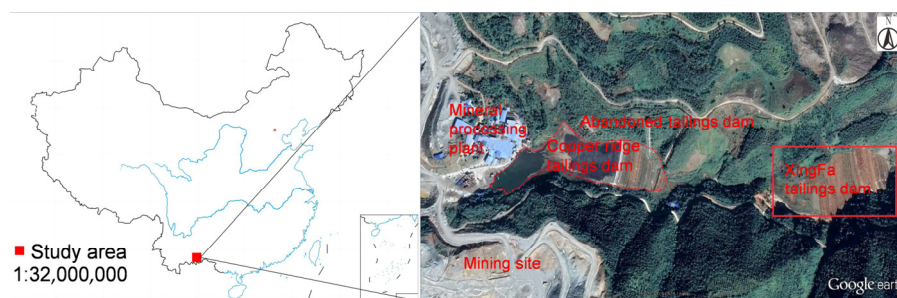


Figure 1. Overview of the study area.

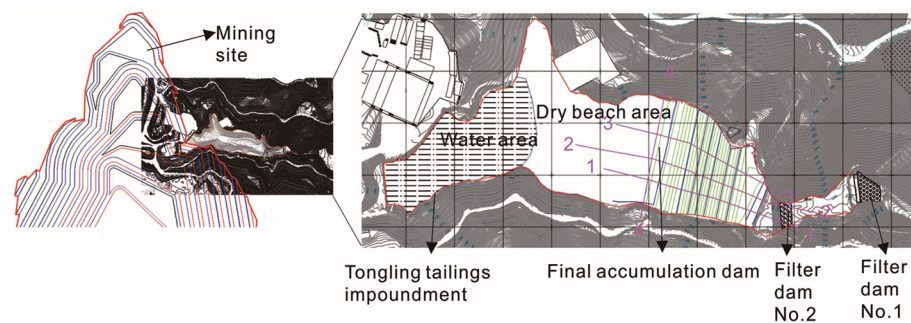


Figure 2. Engineering geological map of the tailings dam (1–4 are section lines).

The initial dam is stacked from an elevation of 1220.0 m. The current tailings elevation is 1255 m, and the stacking dam height is 35 m. Approximately 486,500 m³ of tailings have been stockpiled in the impoundment. There are 27 sub-dams in total. The average slope ratio of the dam is 1:3.0. Moreover, the total storage capacity of impoundment is 540,000 m³. By reviewing China's tailings pond design code, the design grade of the tailings impoundment is fourth class. The tailings impoundment has been used to 1255 m, with 2 m remaining to the design final accumulation elevation of 1257 m. The Tongling tailings impoundment covers an area of approximately 0.038 km², with a dry beach length of approximately 170 m and a water area length of about 120 m.

2.2. Re-Mining Process of the Tailings Dam

Before analyzing and calculating the tailings pond, a detailed survey was launched on site, and samples were brought back for relevant physical and mechanical property analysis. The main components of the tailings are silty clay, silt, and silt sand.

The analysis shows that the materials in the tailings impoundment have a high water content, low strength, and slow percolation under natural conditions.

Combined with the buried depth of the infiltration obtained from the engineering surveys, the tailings impoundment materials are divided into two parts by the infiltration line. These are the unsaturated tailings above the infiltration line and saturated tailings below the infiltration line. In accordance with the current status of the mine and the physical and mechanical properties of the tailings, the unsaturated tailings above the infiltration line in the dry beach area will be recovered by a combination of water gun flushing and a floating sand pumping vessel. In contrast, the saturated tailings below the infiltration line will be recovered by a floating sand pumping vessel.

There are four main stages of the tailings dam recovery process, namely, the current tailings accumulation elevation (1255 m), recovery to half of the dam (1238 m), recovery to the top of the initial dam (1220 m), and recovery to half of the initial dam (1210 m). The subsequent analysis is based on these four stages.

2.3. Stability Analysis Model and Material Parameters

(1) Analysis model

In order to make the results of the subsequent numerical simulation analysis more representative of the overall stability of the tailings pond, the most unfavorable profile for the subsequent analysis was selected, that is, the maximum longitudinal section along the tailings pond trench (as shown in Figure 3). The profile model has a height of 70 m and a length of 360 m. The tailings deposition pattern is coarse at the top and fine at the bottom, and the tailings particle size is coarse before the dam and fine at the end of the dam. The structure of the tailings is heterogeneous and anisotropic. According to the geotechnical engineering investigation report of the tailings pond (Project No.: 15ZG389-PMN-51-0007) and the drilling lithological data, the analysis section was divided into six material zones: silty sand tailing, silty soil tailing, tail silty clay, initial dam, filter dam, and dam foundation (Figure 3).

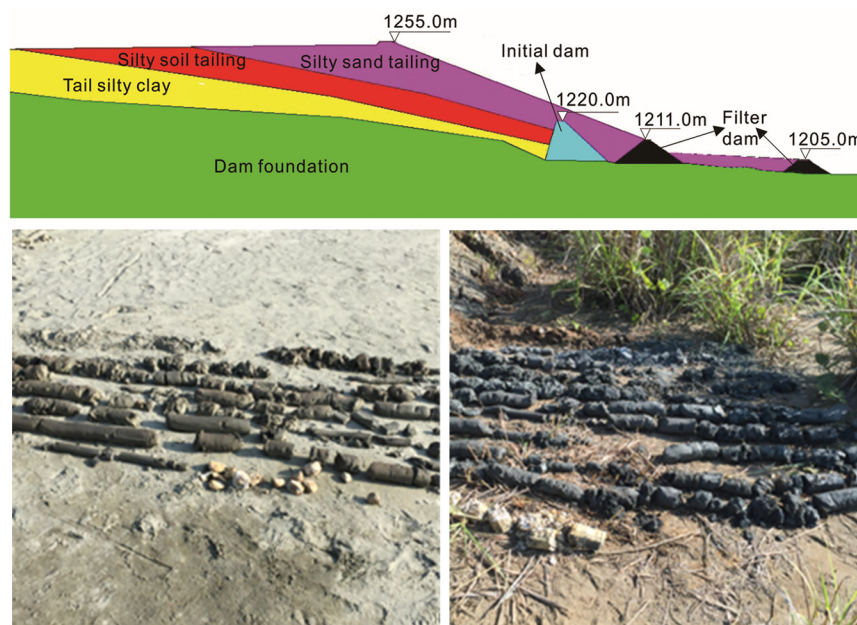


Figure 3. 2-2' Section material division diagram and rock core photograph.

(2) Calculation parameters

In order to ensure that the simulation calculation results are consistent with the actual situation of the mine and to ensure calculation accuracy, it is necessary to select the calculation parameters accurately. A detailed survey of the tailings impoundment was conducted, and multiple representative sampling points were set in the tailings impoundment. A large number of samples (approximately 130 kg) were retrieved. The samples were then processed in strict accordance with the relevant geotechnical test protocols (Figure 4). Soil mechanical tests were launched, such as density tests, tailings consolidation tests, permeability tests, direct shear tests, etc., as shown in Figure 3. After processing the measured data, the simulation calculation parameters of the tailings pond were obtained. In order to ensure the reliability of the data during the tests, multiple parallel tests were carried out for each test. The results are summarized in Table 1. The values of the material parameters for the two-dimensional and three-dimensional analyses are taken strictly from Table 1.

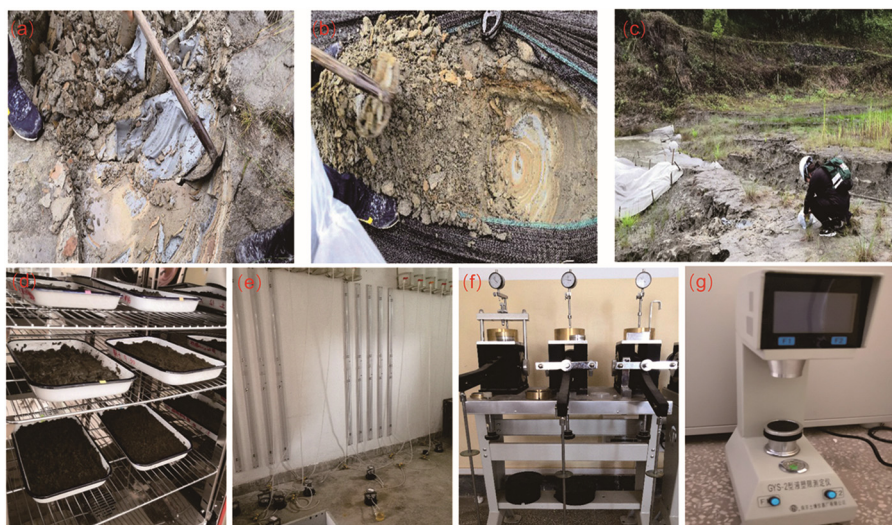


Figure 4. The samples and experiments: (a–c) site sampling; (d–g) laboratory test.

Table 1. Calculation parameter value table.

Materials	Wet Unit Weight γ (KN/m ³)	Modulus of Compressibility E_s	Saturated Unit Weight γ (KN/m ³)	Internal Friction Angle (°)	Cohesive Forces C (KPa)	Osmotic Coefficient (cm/s)
silty sand tailing	21.5	8.41	22.1	28.9	8.1	4.15×10^{-4}
silty soil tailing	18.8	4.04	18.4	18.5	10.0	4.1×10^{-5}
tail silty clay	18.7	3.76	19.0	13.5	12.6	4.5×10^{-5}
initial dam	23.0	3.73	23.0	32.0	120.0	1.0×10^{-6}
filter dam	20.5	–	21.0	30.0	10.0	1.0×10^{-3}
dam foundation	25.6	–	26.0	60.0	100.0	5.2×10^{-5}

2.4. The Basic Principles of Seepage Calculation

2.4.1. Darcy's Law

In 1856, Darcy determined the relationship between seepage velocity (V) and hydraulic slope ($\Delta H/L$) by launching a large number of penetration experiments. Afterwards, the famous Darcy's law was proposed. This law shows that the velocity of water is not only related to the hydraulic gradient but also to the permeability of the soil [46]. Darcy's law is given by Equation (1)

$$V = \frac{Q}{A} = -k \frac{\Delta H}{L} = kJ \quad (1)$$

where V is the flow rate, Q is the flow rate, and A is the section area, which corresponds to the cross-sectional area of the sand column in the experiment. k is the permeability coefficient. ΔH is the head loss, i.e., the difference in head between the upstream and downstream overflow sections. L is the length of the percolation path, and J is the hydraulic gradient. The formula is only proposed for the case of laminar flow. In the operation of the tail mine, the vast majority of seepage is a part of the laminar flow, to which the formula can be applied.

Under rainfall and flood conditions, the shear strength of the tailings will gradually decrease and seepage will gradually cause slip damage to the dam [47]. The initial shear stress of the tailings can be obtained by Equation (2)

$$\tau_c = 0.00821 \gamma R S^{0.040} \left(\frac{\rho_d - \rho}{\rho} \right)^{0.323} \quad (2)$$

where ρ_d is the dry density of the tailings, S is the percentage of clay content, ρ is the density of clear water, and R is the hydraulic radius.

2.4.2. 3D Seepage Field and Stress Field Coupling Principle

(1) The fundamental differential equation for the calculation of 3D steady seepage.

The fundamental differential equation for calculating three-dimensional steady seepage is expressed as Equation (3) [48]

$$\frac{\partial}{\partial x} \left(k_x \frac{\partial h}{\partial x} \right) + \frac{\partial}{\partial y} \left(k_y \frac{\partial h}{\partial y} \right) + \frac{\partial}{\partial z} \left(k_z \frac{\partial h}{\partial z} \right) = 0 \quad (3)$$

where h is the head function, and k_x , k_y , k_z are the permeability coefficients in the x , y , z directions, respectively. The following two types of boundary conditions need to be satisfied for a steady seepage field.

The water head is the first type of boundary condition and is obtained using Equation (4).

$$h|_{\Gamma_1} = h(x, y, z) \quad (4)$$

The flow rate is the second type of boundary condition, is equal to zero, and can be obtained using Equation (5).

$$k_x \frac{\partial h}{\partial x} \cos(n, x) + k_y \frac{\partial h}{\partial y} \cos(n, y) + k_z \frac{\partial h}{\partial z} \cos(n, z)|_{\Gamma_2} = 0 \tag{5}$$

Since the free surface of the seepage is the flow surface, there is no inflow or outflow of flow, so the seepage free surface also needs to satisfy the following conditions, which are given by Equation (6).

$$h = z \tag{6}$$

Γ_1 and Γ_2 constitute the full boundary conditions in the 3D space, and the seepage field inside the tailings dam body can be obtained by solving the finite element equations. (2) Coupling principle of 3D seepage field and stress field.

In MIDAS/GTS, pore water pressure is calculated through seepage analysis to determine fluid permeability. The effect of seepage on stress is mainly realized by applying osmotic force to the soil in seepage. The total stress is divided into effective stress and pore water pressure [49,50]. Since water cannot withstand shear stress, the mechanical effect of effective shear stress is the same as total shear stress, so the total stress expression is assumed as Equation (7).

$$\begin{cases} \sigma_{xx} = \sigma_{xx}' + u_w \\ \sigma_{yy} = \sigma_{yy}' + u_w \\ \sigma_{zz} = \sigma_{zz}' + u_w \\ \tau_{xy} = \tau_{xy}' \\ \tau_{yz} = \tau_{yz}' \\ \tau_{zx} = \tau_{zx}' \end{cases} \tag{7}$$

In the formula, $\sigma_{xx}, \sigma_{yy}, \sigma_{zz}, \sigma_{xy}, \sigma_{yz}, \sigma_{zx}$ are the stress components of a certain point in space, KPa. $\sigma_{xx}', \sigma_{yy}', \sigma_{zz}', \sigma_{xy}', \sigma_{yz}', \sigma_{zx}'$ are the effective stress components at a point in space, KPa. u_w is the pore water pressure, KPa.

The pore water pressure can be divided into steady pore water pressure and excess pore water pressure, which is given by Equation (8)

$$u_w = P_{steady} + P_{excess} \tag{8}$$

where P_{steady} is the steady pore water pressure, KPa. P_{excess} is the excess pore water pressure, KPa. Equation (9) can be obtained from Hooke's law.

$$\begin{pmatrix} \dot{\varepsilon}_x^e & \dot{\varepsilon}_y^e & \dot{\varepsilon}_z^e & \dot{\gamma}_{xy}^e & \dot{\gamma}_{yz}^e & \dot{\gamma}_{zx}^e \end{pmatrix}^T = \frac{1}{E} \begin{pmatrix} 1 & -\nu & -\nu & 0 & 0 & 0 \\ -\nu & 1 & -\nu & 0 & 0 & 0 \\ -\nu & -\nu & 1 & 0 & 0 & 0 \\ 0 & 0 & 0 & 2 + 2\nu & 0 & 0 \\ 0 & 0 & 0 & 0 & 2 + 2\nu & 0 \\ 0 & 0 & 0 & 0 & 0 & 2 + 2\nu \end{pmatrix} \begin{pmatrix} \dot{\sigma}_{xx}' \\ \dot{\sigma}_{yy}' \\ \dot{\sigma}_{zz}' \\ \dot{\sigma}_{xy}' \\ \dot{\sigma}_{yz}' \\ \dot{\sigma}_{zx}' \end{pmatrix} \tag{9}$$

E is Elastic Modulus, MPa. ν is the Poisson's ratio of the material. $\varepsilon_x, \varepsilon_y, \varepsilon_z, \gamma_{xy}, \gamma_{yz}, \gamma_{zx}$ are the line and tangential strains at any point in space.

In Formula (7), the steady pore water pressure is determined by the height of the underground water level, and its derivative is zero. Equation (10) can be obtained.

$$\dot{u}_w = \dot{P}_{excess} \tag{10}$$

According to Formulas (7) and (10), Formula (9) can be solved. The stress and strain state of any point in the tailings dam can be obtained by solving Formula (11).

$$\begin{pmatrix} \dot{\varepsilon}_x^e \\ \dot{\varepsilon}_y^e \\ \dot{\varepsilon}_z^e \\ \dot{\gamma}_{xy}^e \\ \dot{\gamma}_{yz}^e \\ \dot{\gamma}_{zx}^e \end{pmatrix} = \frac{1}{E} \begin{pmatrix} 1 & -\nu & -\nu & 0 & 0 & 0 \\ -\nu & 1 & -\nu & 0 & 0 & 0 \\ -\nu & -\nu & 1 & 0 & 0 & 0 \\ 0 & 0 & 0 & 2+2\nu & 0 & 0 \\ 0 & 0 & 0 & 0 & 2+2\nu & 0 \\ 0 & 0 & 0 & 0 & 0 & 2+2\nu \end{pmatrix} \begin{pmatrix} \dot{\sigma}_x - \dot{P}_{excess} \\ \dot{\sigma}_y - \dot{P}_{excess} \\ \dot{\sigma}_z - \dot{P}_{excess} \\ \dot{\tau}_{xy} \\ \dot{\tau}_{yz} \\ \dot{\tau}_{xz} \end{pmatrix} \quad (11)$$

2.5. Two-Dimensional Seepage Analysis of the Tailings Dam

2.5.1. Analysis of Dam Infiltration Lines at Different Elevations

The height of the tailings dam and the length of the dry beach in tailings impoundment design are related to the infiltration line, which is the lifeline directly related to the safety of the tailings dam. In the process of mining tailings, with the change of the dam height, the dry beach length is also changed, thus affecting the position of the infiltration line. The variation of the infiltration line under different stoping elevations was analyzed, and the seepage characteristics of the tailings pond under various working conditions, which can provide a reference for subsequent stability calculations, was also determined.

The infiltration line is generally obtained by field measurements, and the defective part of the field measurement is acquired by seepage calculations. The numerical simulation is performed using two-dimensional software based on the infiltration lines actually measured in the field. During the calculations, it was assumed that the upstream water level of the tailings pond and the downstream water level remained constant for a short period, therefore, the seepage analysis was performed as a steady flow. In order to make the calculation results closer to reality, the calculation result is modified according to the survey data of the field infiltration line.

2.5.2. Two-Dimensional Stability Analysis of Dams

Based on the above infiltration line analysis results, the limit equilibrium method was used [51,52] to analyze the effects of different elevations and working conditions on the stability of the dam body during the stoping process of the tailings impoundment. The different recovery heights are equivalent to the four different recovery heights in the infiltration line analysis. Southwest China is an earthquake-prone region, therefore, earthquake influence should be considered in dam stability analyses. (According to the engineering survey data, the earthquake fortification intensity of the area is 6 degrees, and the design basic acceleration of ground motion value of the site is 0.05 g.)

The stability analysis takes into account three main operating conditions: ① The steady infiltration pressure at the normal reservoir level, the self-weight of the dam, and the pore water pressure in the foundation of the dam (normal working conditions); ② The self-weight, the pore water pressure in the dam foundation, and the potential for stable infiltration pressure at the design flood level (flood working conditions); ③ The infiltration pressure at the normal reservoir level, the self-weight of the dam, the pore water pressure in the dam and foundation, and seismic loading (special working conditions).

2.6. 3D Stability Analysis of the Tailings Dam under Different Working Conditions

The stability analysis was conducted at different elevations by means of a two-dimensional analysis. However, the stress and displacement changes within the tailings impoundment during the operation cannot be derived from the two-dimensional analysis. Therefore, in order to further determine the variation of the stress and displacement fields in the tailings pond, a three-dimensional analysis of the tailings pond was launched. 3Dmine software was used to create the 3D surface structure of the tailings impoundment, and then

a 3D numerical analysis model was established by means of Midas GTS NX software 2023 v1.1. There are two main approaches: ① If the object of the analysis is regular, the terrain conditions are relatively simple, and the terrain fluctuation is not large, the object profile can be analyzed directly for lateral stretching to generate 3D entities; ② When the object of the analysis is located in complex terrain, the terrain is significantly undulating, and the object of the analysis is irregular. Firstly, it is necessary to generate a realistic ground surface with 3Dmine software and then couple it with Midas GTS NX numerical simulation software to generate a more realistic 3D entity for analysis. A combination of two three-dimensional analyses was used to make the analysis more comprehensive. The Midas GTS NX numerical simulation software was selected to carry out the analysis.

2.6.1. Three-Dimensional Static Analysis of the Tailings Impoundment

Four different stopping heights were selected to conduct a three-dimensional static analysis of the tailings impoundment. The overall displacement variation of the tailings impoundment in the process of mining was analyzed. The tailings dam model has a length of 690 m, a width of 370 m, and a height of 90 m. The grid cell size is 5 m, and the model has 97,328 cells and 54,654 nodes. Figure 5 presents the calculation model.

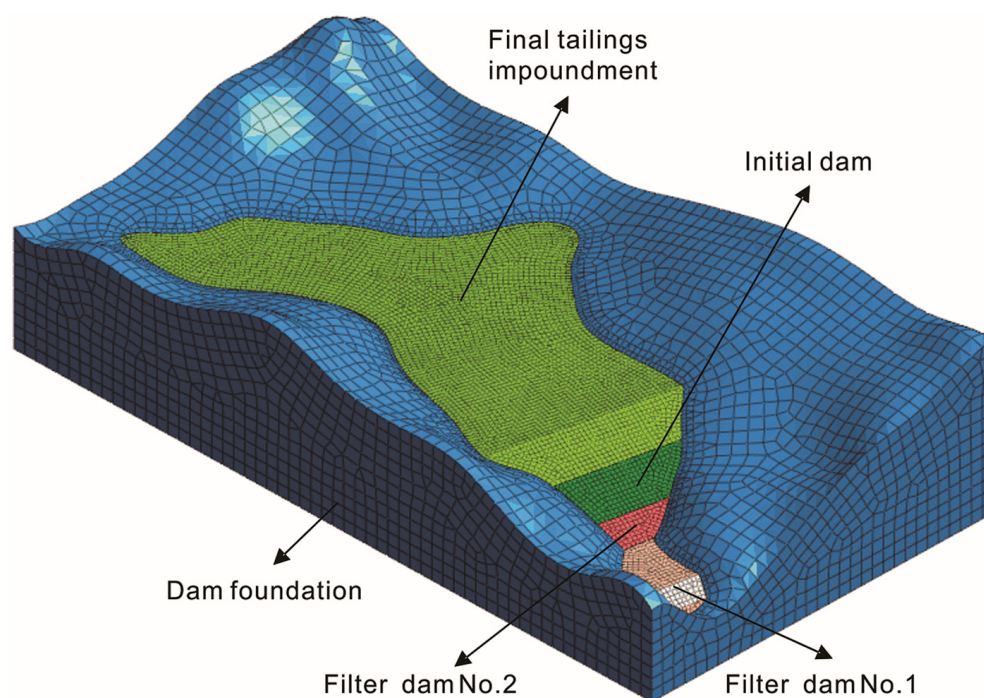


Figure 5. Calculation model diagram.

2.6.2. Three-Dimensional Stability Analysis of the Tailings Impoundment under Different Working Conditions

(1) Establishment of the 3D model

Due to the low depression in the middle of the tailings impoundment, the surrounding terrain fluctuates wildly. In the three-dimensional analysis, due to avoiding software focus on the surrounding high and steep mountains, the accuracy of the tailings pond area cannot be guaranteed. The dam body at the highest elevation of the tailings impoundment (1255.0 m) was selected as the analysis model, and a 3D solid was generated from the calculated profile. The model has a length of 360 m, a width of 80 m, and a height of 80 m. The grid cell size is 5 m, and the model has 13,472 cells and 15,283 nodes (Figure 6).

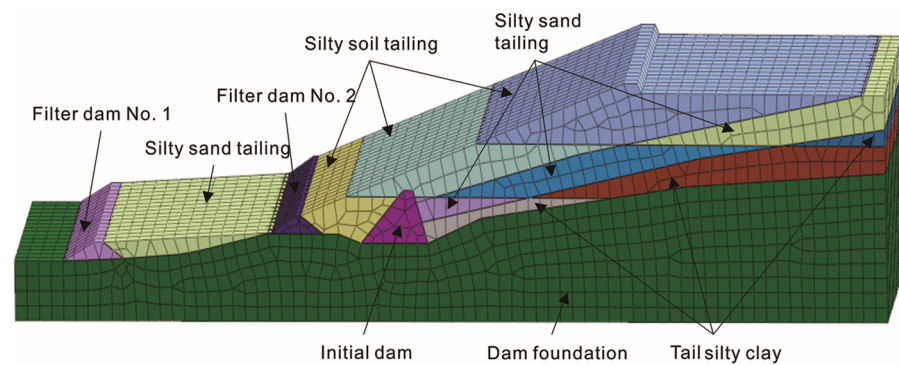


Figure 6. Three-dimensional stability calculation model of the dam.

The MIDAS GTS NX software has a variety of constitutive models, and the Mohr–Coulomb constitutive model was chosen. Choosing an appropriate constitutive model for numerical simulation analysis of tailings impoundment is crucial. This is because, under normal conditions, the stress and strain interactions among tailings are complex, with nonlinear, elasto-plastic, dilatant, and anisotropic physical properties being common. The rationality of the selection of the constitutive model is directly related to the accuracy of the numerical simulation calculations. However, current research does not yet provide a constitutive model for tailings soil that accurately reflects all conditions; most existing models apply only to tailings soil under certain specific conditions. With the deepening of research on finite element technology, research on the constitutive models of geotechnical bodies has greatly improved, and the accuracy of analysis and calculation has also become higher.

This study chose the Mohr–Coulomb model for numerical analysis. The main advantages and disadvantages of this model can be summarized as follows:

(1) The main advantages of the Mohr–Coulomb model are:

(a) Accuracy: the Mohr–Coulomb constitutive model is an empirical clay behavior model, which can be understood as a mixture of perfectly plastic behavior and linear elasto-plasticity. Hence, it is more accurate than linear elastic models in describing the nonlinear behavior of soil;

(b) Applicability: the Mohr–Coulomb model applies to various soil conditions (dry, wet, saturated, etc.) and soil types (sand, clay, etc.), making it broadly applicable in practical engineering. In this study, the tailings consist primarily of clay tailings and sand tailings. Hence, the Mohr–Coulomb model can effectively reflect the dam’s stability under intense rainfall and flooding;

(c) Completeness: the Mohr–Coulomb theory considers both normal stress and shear stress, thus evaluating material resistance to damage more comprehensively;

(2) The main disadvantages of the Mohr–Coulomb model are:

(a) Parameter selection: choosing the Mohr–Coulomb parameters is essential but can sometimes pose difficulties. The accuracy of the parameter selection directly influences the analysis results’ accuracy;

(b) Practical problems: the Mohr–Coulomb model might not suit all types of soil. For instance, the Mohr–Coulomb model may not accurately predict the behavior of highly plastic clay or very soft soils.

In this study, the tailings and dam body did not involve highly plastic clay and soft soil. The tailings soil body was mainly composed of powdery clay tailings and sand tailings. Therefore, based on the actual situation of the tailings impoundment and considering the applicability and disadvantages of the Mohr–Coulomb model, this study chooses this model to more accurately reflect the constitutive behavior of the studied subject.

The strength reduction method (SRM) was selected as the stability analysis method of the 3D model.

(2) The calculation conditions of the 3D model

Four analysis conditions were comprehensively considered according to the actual conditions and the two-dimensional analysis conditions: ① Working condition 1 is the normal water level; ② Working condition 2 is the flood level; ③ Working condition 3 is a combination of flooding and heavy rainfall (special working condition I); ④ Working condition 4 is a combination of flooding and an earthquake (special working condition II). The earthquake fortification intensity and the design basic acceleration of ground motion value are consistent with the two-dimensional analysis.

The values of each material parameter are shown in Table 1. The calculated values of the safety factors for different operating conditions are summarized in Table 2.

Table 2. Safety factors under different working conditions.

Working Condition	Calculated Safety Factor	Minimum Safety Coefficient Allowed by Code	Whether Safety Requirements Are Met
Normal	1.4630	1.45	Yes
Flooding	1.4375	1.1~1.2	Yes
Special I	1.3625	1.05~1.10	Yes
Special II	1.3373	1.05	Yes

In analyzing and comparing the research materials on the stability of valley-type tailings dams from other regions, it has been found that floods, rainfall, and earthquakes are the primary factors affecting the stability of such reservoirs. Due to their unique terrain and geological conditions, as well as hydrological and meteorological conditions and ecological environment, valley-type tailings dams present a high safety risk. Floods may lead to scouring and landslides of the dam, and inadequate spillway facilities or blockages may trigger overtopping due to floods. Rainwater infiltration leads to the rise of the saturation line, which in turn decreases the stability and strength of the dam and increases the risk of landslides. Earthquakes can cause geological disasters and landslides or collapses of the dam, threatening the safety of the tailings dam.

The safety of tailings dams mainly depends on whether the safety factor is reduced, whether the displacement amount is large, and whether the penetration range of equivalent plastic area is expanded. By comparing the results of 3D stability and the critical safety factor, it is clear that the overall dam displacement decreased with the recovery height in the static analysis. Under the different analysis conditions, the dams are subject to small displacements, and the strains all occur on the outer slope of the tailings dam. Under flood and heavy rainfall conditions, the silty sand tailing becomes saturated, increasing the dam's self-weight and leading to a lack of slip resistance. A saturated silty sand tailing will have low strength and poor consolidation and will liquefy during seismic events. Therefore, there is a certain zone of plastic deformation inside the reservoir under seismic conditions, which occurs from the top of the initial dam to the middle of the stacked dam.

3. Results

3.1. Variation of the Infiltration Line of the Tailings Dam

By performing seepage calculations on the tailings dam body, the variation law of the infiltration line of the dam in the process of mining is observed. Figures 7 and 8 show the results of the infiltration line calculations for tailings dam with different mining heights.

In Figures 7 and 8, a presents the tailings dam elevation, b presents the initial dam, c presents filter dam no. 2, d presents the saturation line, e presents filter dam no. 1, f presents the tailings dry beach.

From the above calculations, it can be seen that the calculated infiltration line is substantially similar to the field exploration infiltration line. Since the calculation of the infiltration line combines different working conditions, it more comprehensively reflects the stability of the tailings. The dam elevation has a significant influence on the buried depth of the saturation line. The infiltration line is significantly higher under flood conditions

indicating that flooding has a more significant impact on the stability of the tailings dam. Under flood conditions, the tailing sands gradually saturate. Under the action of seepage, the pore water pressure within the soil decreases, and the shear strength subsequently decreases, which can cause infiltration damage to the tailing dam body.

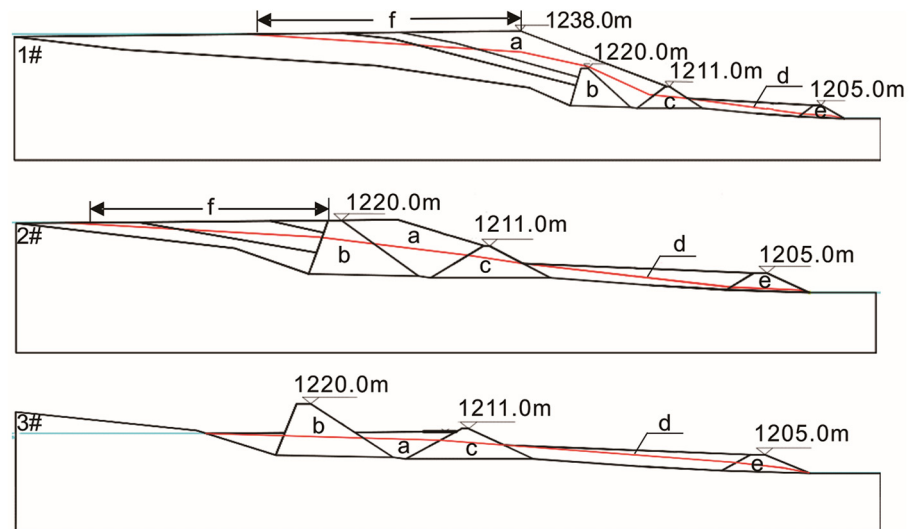


Figure 7. Seepage calculation (normal working conditions): 1# the dam elevation is 1238 m, 2# the dam elevation is 1220 m, 3# the dam elevation is 1211 m.

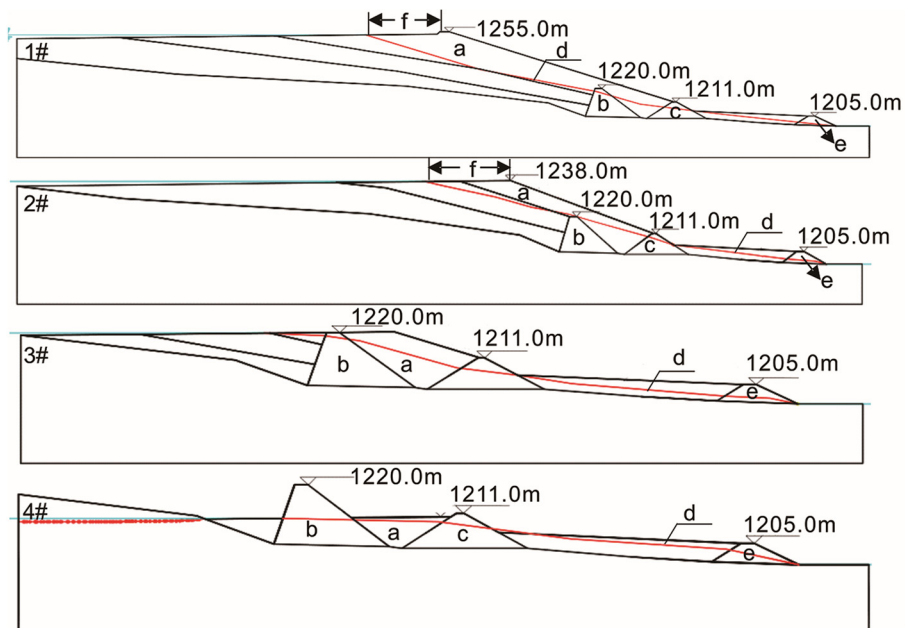


Figure 8. Seepage calculation (flooding conditions): 1# the dam elevation is 1255 m, 2# the dam elevation is 1238 m, 3# the dam elevation is 1220 m, 4# the dam elevation is 1211 m.

With the advancement of the re-mining process, the elevation of the tailings dam gradually decreases, the infiltration line is reduced, and the length of the dry beach is also shortened. This is due to the gradual reduction in tailings and industrial waste in the impoundment during the recovery process, influenced by the deposition pattern of tailing sand in the reservoir area. The particles of the tailings deposit on the beach successively change from coarse to fine going from the near to the far end. As a result, the permeability of the infiltration line from the beginning to the end changes from small to large.

3.2. Two-Dimensional Stability

Due to the limited space available, the safety factors for the different operating conditions in the recovery process are summarized in Table 3. The calculated values are compared with the minimum permissible safety factors required by the code.

Table 3. Calculation results of dam stability.

Tailings Dam Elevation (m)	Working Conditions	Calculated Safety Factor	Circle Arc Sliding Radius (m)	Minimum Safety Factor Allowed by Code
1255	Normal	1.238	134.574	1.15
	Flooding	1.195	133.400	1.05
	Special	1.174	132.651	1.00
1238	Normal	1.670	140.594	1.15
	Flooding	1.621	140.594	1.05
	Special	1.596	140.594	1.00
1220	Normal	1.910	60.384	1.15
	Flooding	1.864	60.384	1.05
	Special	1.835	30.491	1.00
1210	Normal	3.202	28.258	1.15
	Flooding	3.131	28.258	1.05
	Special	3.020	28.258	1.00

The accumulation elevation of the tailings pond gradually decreases during the recovery process, the accumulation in the dam gradually reduces, and the total self-weight of the tailings pond decreases. The infiltration line is directly proportional to the recovery and accumulation elevations in the previous section. Under each working condition, the safety factor is inversely proportional to the accumulation elevation, and the safety factor gradually rises with the elevation reduction. The overall relationship between the safety factor value of the three operating conditions is normal working conditions > flood working conditions > special (earthquake) working conditions (Figure 9).

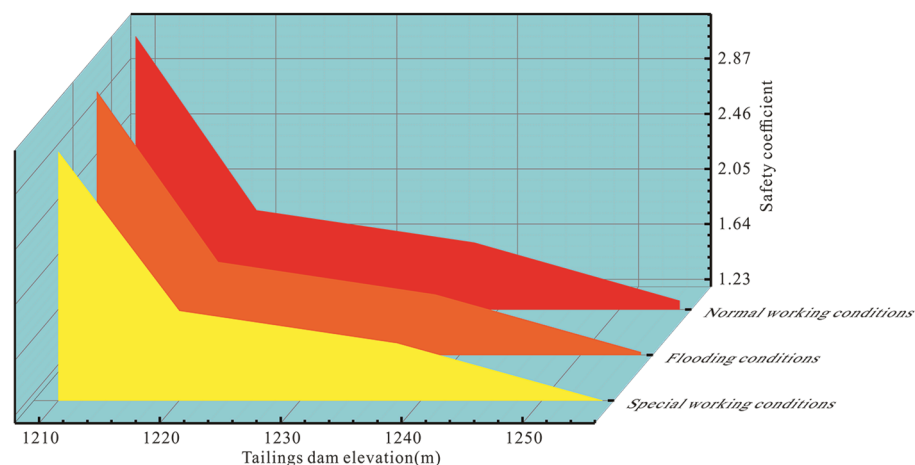


Figure 9. Change of dam safety coefficient.

3.3. Three-Dimensional Stability

3.3.1. Statical Analysis Results

At the elevation stage of 1255 m–1238 m, the minimum principal stress, the maximum principal stress, and the maximum shear stress are all positive values (Figure 10). There is both tensile and compressive stress at this stage, which is mainly concentrated in the tailings reservoir area. The maximum shear stress decreases in a laminar pattern from

bottom to top in the reservoir area, indicating that the shear stress is mainly influenced by self-weight.

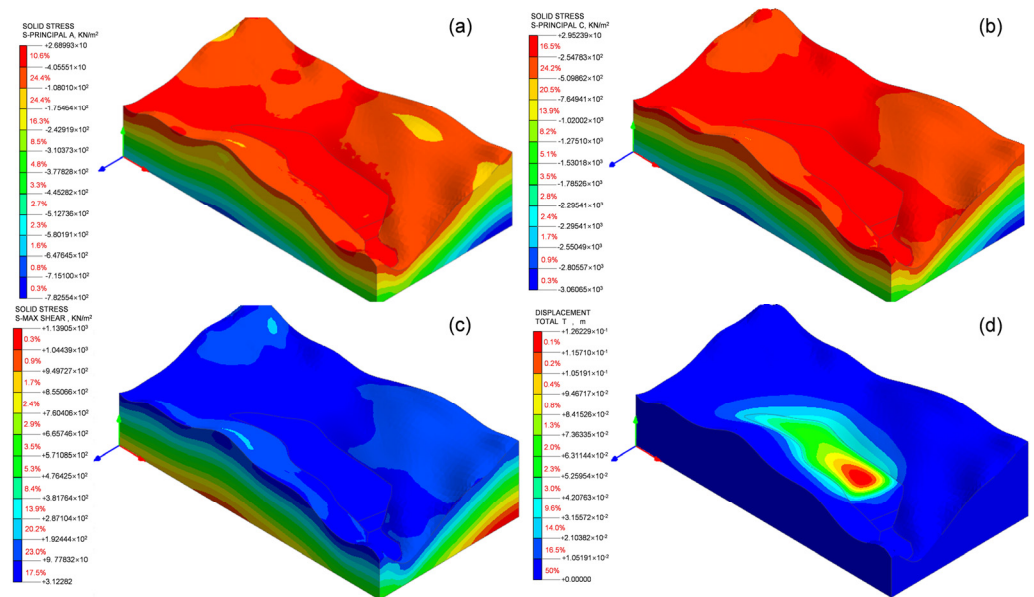


Figure 10. The calculation of 1255 m–1238 m: (a) the minimum principal stress cloud atlas, (b) the maximum principal stress cloud atlas, (c) the maximum shear stress cloud atlas, (d) the excursion cloud atlas.

When mining to the crest of the initial dam, the minimum principal stress and the maximum shear stress are positive, and the maximum principal stress is negative, indicating that there is tensile stress in the reservoir area. The maximum shear stress decreases in a laminar pattern from bottom to top in the reservoir area, indicating that the shear stress is mainly influenced by self-weight. After mining, small displacement changes will occur in the dam, mainly occurring in the position of the tailings impoundment (Figure 11).

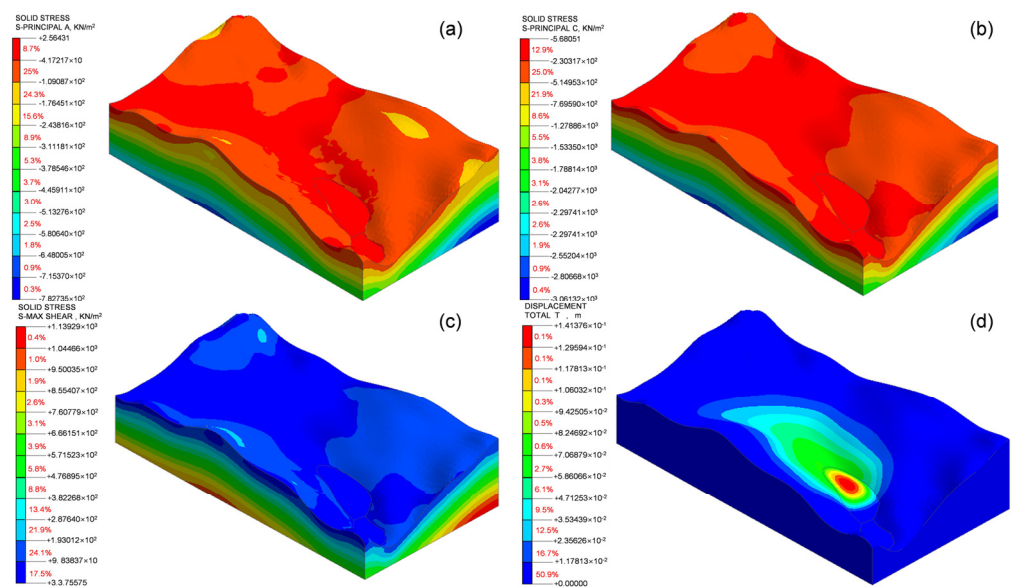


Figure 11. The calculation of 1238 m–1220 m: (a) the minimum principal stress cloud atlas, (b) the maximum principal stress cloud atlas, (c) the maximum shear stress cloud atlas, (d) the excursion cloud atlas.

At the elevation stage of 1220 m–1211 m, the maximum shear stress is in the upper part of the dam, where the shear stress is minimal and gradually increases in the direction of the ground in a laminar pattern (Figure 12). The shear stress is mainly influenced by self-weight. After stoping, the displacement is 0.095 m, which may be caused by the fact that the actual flushing production cannot be determined by the water gun flushing method.

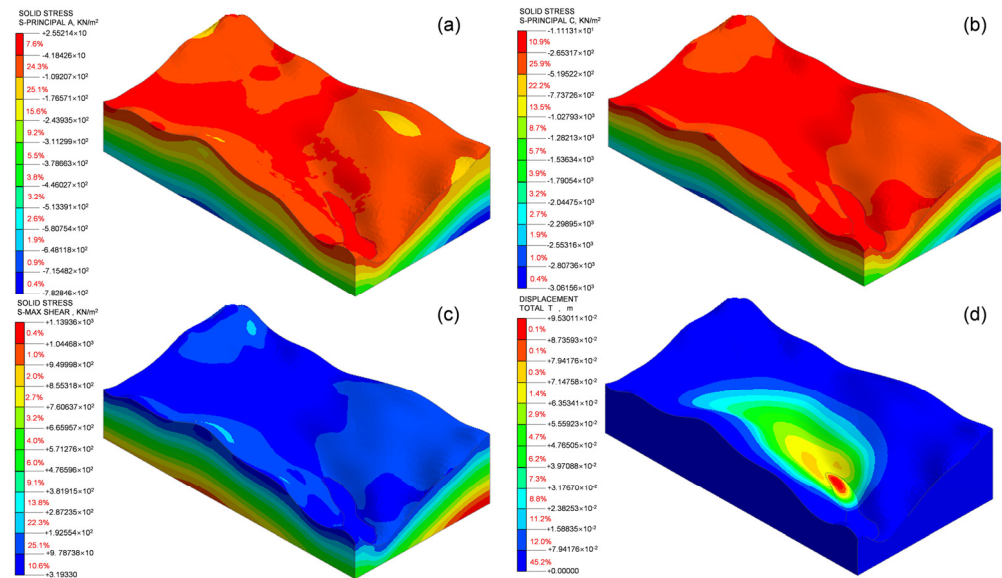


Figure 12. The calculation of 1220 m–1211 m: (a) the minimum principal stress cloud atlas, (b) the maximum principal stress cloud atlas, (c) the maximum shear stress cloud atlas, (d) the excursion cloud atlas.

During the mining process, the tailings dam gradually decreases from 1255 m to 1211 m, and the displacement mainly occurs in the middle of the tailings dam. The displacement decreases from 0.126 m to 0.095 m, the total displacement is small, and the tailings dam foundation can remain stable during the whole mining process. The tailings pond is mainly affected by compressive stresses generated by self-weight. Although there is a certain displacement, considering that the actual construction method of the reservoir is hydraulic mining, the displacement is negligible.

3.3.2. 3D stability Analysis Results under Diverse Analysis Conditions

(1) Normal working conditions

Under normal conditions, the safety factor value of the strength reduction calculation is 1.4630. The total displacement is mainly at the dam top. The amount is 0.443 m, which is slightly larger than the static analysis. The maximum shear strain and the equivalent plastic strain under these conditions are found to be in approximately the same location. The maximum shear stress and equivalent plastic strain diagrams reveal that the main strain is at the back end of filter dam no. 2, where the deformation is small (Figure 13).

(2) Flooding conditions

Under flooding conditions, the safety factor value of the strength reduction calculation is 1.4375. The value of the safety factor is lower than the normal working conditions, and the total displacement is about 0.305 m. According to the equivalent plastic strain cloud atlas, it was found that there is a particular plastic deformation zone on the front slope of the dam, and that the excessive region of the equivalent plastic strain becomes more prominent, which may lead to slip failure (Figure 14).

(3) Special working conditions I: flood + heavy rainfall

The safety factor value of the strength reduction calculation is 1.3625 under the special working conditions I. The total displacement mainly occurs at the top of the dam. The amount of the displacement is 0.268 m. The equivalent plastic strain zone mainly occurs at

filtration dam no. 2 and in the lower area of the dam crest, where the strain zone is larger, and the safety factor is reduced (Figure 15).

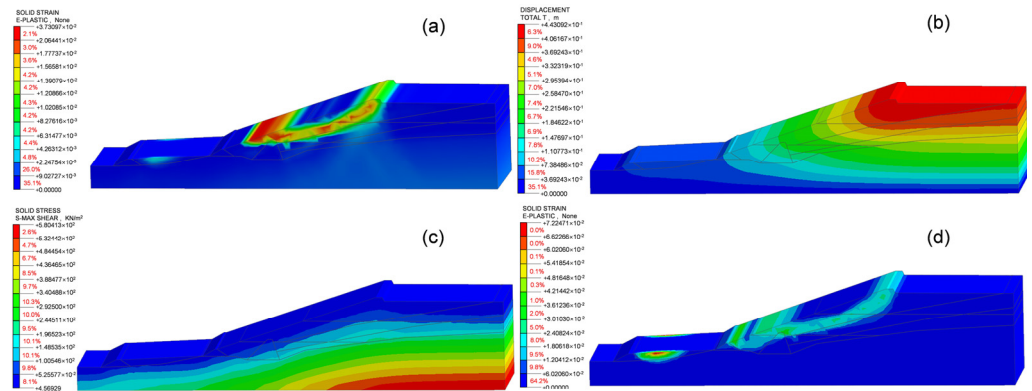


Figure 13. (a) The safety factor cloud atlas, (b) the excursion cloud atlas, (c) the maximum shear stress cloud atlas, (d) the equivalent plastic strain cloud atlas.

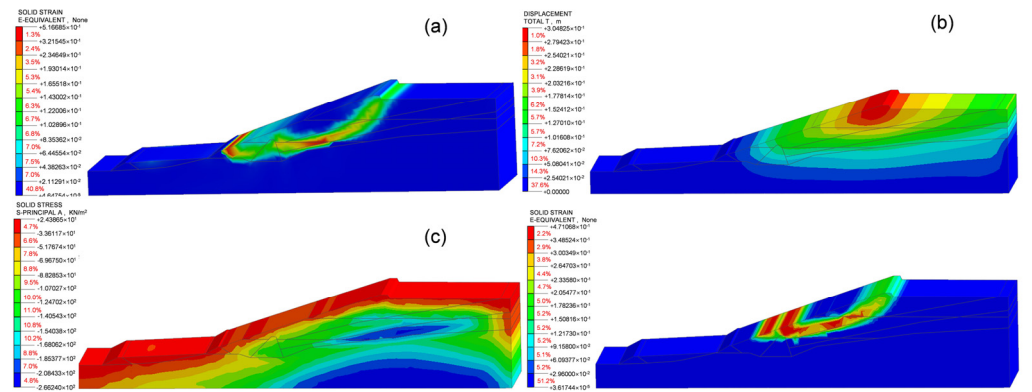


Figure 14. (a) The safety factor cloud atlas, (b) the excursion cloud atlas, (c) the maximum principal stress cloud atlas, (d) the Equivalent plastic strain cloud atlas.

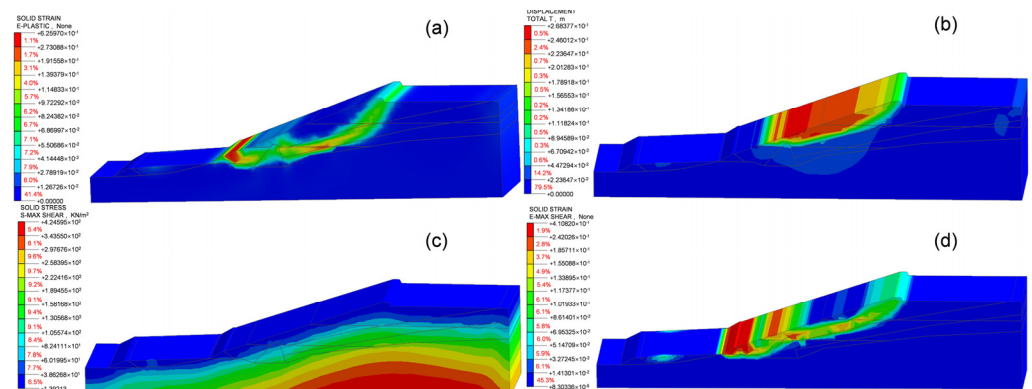


Figure 15. (a) The safety factor cloud atlas, (b) the excursion cloud atlas, (c) the maximum shear stress cloud atlas, (d) the Equivalent plastic strain cloud atlas.

(4) Special working conditions II: flood + earthquake

The safety factor value of the strength reduction calculation is 1.3373 under special working conditions II. Under earthquake conditions, the shear stress in the dam changes, and a partial plastic deformation zone is generated inside the dam. The deformation zone runs from the initial dam position to the tail of the dam body, and the penetration area is expanded (Figure 16).

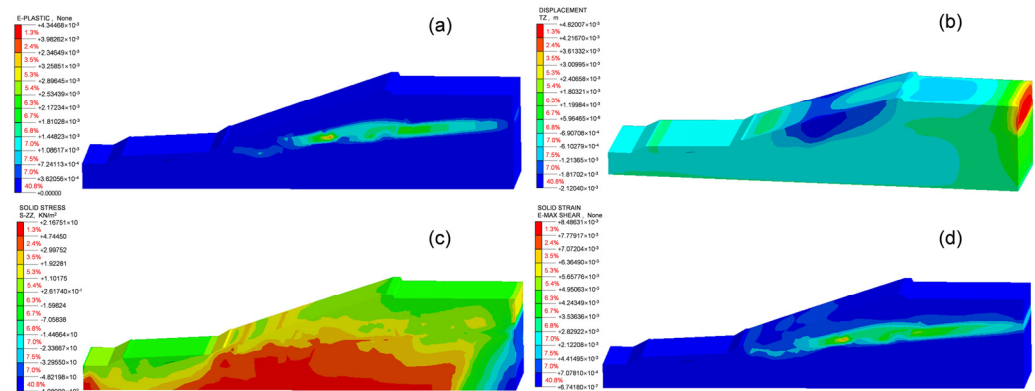


Figure 16. (a) The safety factor cloud atlas, (b) the maximum principal stress cloud atlas, (c) the maximum shear stress cloud atlas, (d) the Equivalent plastic strain cloud atlas.

4. Discussion

Research on tailings dam re-mining at home and abroad has mainly focused on the replacement of re-mining methods, re-mining equipment, reclamation technology, and the use of tailings to fill the void area. A comprehensive analysis of the tailings pond around the stability evolution characteristics of the tailings dam during the re-mining process is presented to ensure the stability of the tailings dam and the safety of the staff during the re-mining process. A seepage analysis model at different elevations was established, and seepage and infiltration line change patterns from an actual 3D ground surface were analyzed. Four typical retrieval elevations were selected, and various analytical conditions were considered by means of 2D and 3D numerical simulations. The research reveals the pattern of the interaction between the recovery elevation and the analyzed working conditions. The results provide a deeper insight into the changes in the stress field, seepage field, and displacement field of the tailings impoundment during the recovery process, which may help us carry out dam safety monitoring and early warning and forecasting and provide a theoretical basis for the actual construction of the mine.

In the two-dimensional numerical simulation, the dam body was simplified, and the physical and mechanical parameters were somewhat modified according to the engineering survey data. The infiltration line calculated by the two-dimensional software has also been amended. The surrounding geological environment of the tailings impoundment was simplified in the 3D morphing, and the boundary conditions were set slightly differently from the actual situation, which may lead to some specific errors. In future studies, it should be modified and modeled according to the current situation.

Tailings impoundment retrieval is a dynamic process, and only four typical retrieval heights were analyzed, failing to take any one height into account to calculate its stability. Therefore, a dynamic simulation of the whole retrieval process should be achieved in our subsequent study.

5. Conclusions

A combination of field investigation, laboratory tests, seepage theory analysis, and numerical simulation was used to study the stability of dams with different stopping elevations in the Tongling valley-type tailings impoundment. Based on the actual situation of the mining area and the calculation, the following conclusions can be drawn.

(1) In the stopping process, different elevations significantly influence the burial depth of the saturation line. The lower the retrieval height, the deeper the infiltration line is buried, which is beneficial to the dam's stability. However, at the same elevation, a small portion of the infiltration line will overflow under flood conditions, mainly because the tailings pond has been out of service for many years and the relevant drainage facilities have not been repaired and unclogged for many years, resulting in the poor drainage capacity of the dam, which leads to an apparent uplift of the infiltration line under flood

conditions. Therefore, before mining the tailings pond in the current project, the drainage facilities should undergo maintenance, and the drainage device should be dredged to ensure the stability of the tailings dam during the mining process.

(2) The recovery of tailings ponds is a slow load-shedding process. In the limit equilibrium analysis, the safety factor increases with the decrease in mining height. The coefficient of the safety of the dam under different working conditions is greater than the minimum value allowed by the code, and the dam is always in a steady condition during the retrieval process. In the three-dimensional static analysis, the higher the dam elevation, the greater the overall displacement of the tailings pond and the more detrimental it is to the stability of the dam.

(3) The more extreme the analysis, the less safe the dam. Under extreme working conditions, the shear stress inside the dam will switch, the shear strength of the dam will be reduced, and the safety coefficient will decrease too. The equivalent plastic zone will also expand through the scope. There is an apparent continuous slip surface within the tailings dam, particularly under seismic conditions. However, under the various working conditions, the tailing pond is able to meet the requirements for dam body stability and fulfill the conditions for safe production.

(4) The method developed in the study centers around numerical simulation, which allows the researchers to assess the potential risks and outcomes related to the stability of tailings dams during the recovery process. The use of 2D software assists in determining the position of the tailings dam infiltration line and the changes in the dam safety factor during the stopping process. The study also incorporates 3D mapping of the tailings impoundment with 3Dmine software, enabling a more comprehensive 3D numerical analysis model established through Midas GTS NX software. Combining these processes provides them with a clear visual and numerical representation of the impoundment's state. This technology-supported approach has many potential applications around the world, especially in regions where tailings dam failure could pose significant environmental and human risks. Therefore, this study presents not only a promising avenue for the management and recovery of tailings impoundments but also highlights the pressing need to incorporate technology into our environmental management strategies.

Author Contributions: Conceptualization, Y.P. and J.C.; methodology, Y.P.; software, Y.P.; validation, Y.P., J.C. and X.Z.; formal analysis, Y.P.; investigation, Y.P.; resources, X.Z.; data curation, Y.P.; writing—original draft preparation, Y.P.; writing—review and editing, Y.P., J.C., C.Z., X.Z. and S.W.; visualization, Y.P.; supervision, Y.P., J.C., C.Z., X.Z. and S.W.; project administration, J.C.; funding acquisition, J.C. All authors have read and agreed to the published version of the manuscript.

Funding: This research is financially supported by the National Natural Science Foundation of China joint research program of Yunnan (grant No. U1502231), and Geological Survey of China (Grant No. DD20221645).

Data Availability Statement: Not applicable.

Acknowledgments: The authors are grateful for the helpful comments from many researchers and colleagues.

Conflicts of Interest: The author declare no conflict of interest.

References

1. Dong, L.; Deng, S.; Wang, F. Some developments and new insights for environmental sustainability and disaster control of tailings dam. *J. Clean. Prod.* **2020**, *269*, 122270. [[CrossRef](#)]
2. Hatje, V.; Pedreira, R.M.; de Rezende, C.E.; Schettini, C.A.F.; de Souza, G.C.; Marin, D.C.; Hackspacher, P.C. The environmental impacts of one of the largest tailing dam failures worldwide. *Sci. Rep.* **2017**, *7*, 10706. [[CrossRef](#)] [[PubMed](#)]
3. Tian, S.; Chen, J.-h. Multi-hierarchical fuzzy judgment and nested dominance relation of rough set theory-based environmental risk evaluation for tailings reservoirs. *J. Cent. S. Univ.* **2015**, *22*, 4797–4806. [[CrossRef](#)]
4. Yang, Y.; Wei, Z.; Cao, G.; Yang, Y.; Wang, H.; Zhuang, S.; Lu, T. A case study on utilizing geotextile tubes for tailings dams construction in China. *Geotext. Geomembr.* **2019**, *47*, 187–192. [[CrossRef](#)]

5. Yin, G.; Li, G.; Wei, Z.; Wan, L.; Shui, G.; Jing, X. Stability analysis of a copper tailings dam via laboratory model tests: A Chinese case study. *Miner. Eng.* **2011**, *24*, 122–130. [[CrossRef](#)]
6. Edraki, M.; Baumgartl, T.; Manlapig, E.; Bradshaw, D.; Franks, D.M.; Moran, C.J. Designing mine tailings for better environmental, social and economic outcomes: A review of alternative approaches. *J. Clean. Prod.* **2014**, *84*, 411–420. [[CrossRef](#)]
7. He, Y.; Li, B.-b.; Zhang, K.-n.; Li, Z.; Chen, Y.-g.; Ye, W.-m. Experimental and numerical study on heavy metal contaminant migration and retention behavior of engineered barrier in tailings pond. *Environ. Pollut.* **2019**, *252*, 1010–1018. [[CrossRef](#)]
8. He, Z.-b.; Liao, T.; Liu, Y.-g.; Xiao, Y.; Li, T.-t.; Wang, H. Influence of sulfur addition/solids content ratio on removal of heavy metals from mine tailings by bioleaching. *J. Cent. S. Univ.* **2012**, *19*, 3540–3545. [[CrossRef](#)]
9. Salam, S.; Xiao, M.; Khosravifar, A.; Ziotopoulou, K. Seismic stability of coal tailings dams with spatially variable and liquefiable coal tailings using pore pressure plasticity models. *Comput. Geotech.* **2021**, *132*, 104017. [[CrossRef](#)]
10. Zhang, Z.; Zhang, S. A new method of coal fine particles humidification and agglomeration: Synergistic dust suppression with composition of soap solution. *Process Saf. Environ. Prot.* **2022**, *159*, 146–156. [[CrossRef](#)]
11. Tian, S.; Dai, X.; Wang, G.; Lu, Y.; Chen, J. Formation and evolution characteristics of dam breach and tailings flow from dam failure: An experimental study. *Nat. Hazards* **2021**, *107*, 1621–1638. [[CrossRef](#)]
12. Wu, T.; Qin, J. Experimental study of a tailings impoundment dam failure due to overtopping. *Mine Water Environ.* **2018**, *37*, 272–280. [[CrossRef](#)]
13. Xu, W.-b.; Liu, B.; Wu, W.-l. Strength and deformation behaviors of cemented tailings backfill under triaxial compression. *J. Cent. S. Univ.* **2020**, *27*, 3531–3543. [[CrossRef](#)]
14. Luino, F.; De Graff, J.V. The Stava mudflow of 19 July 1985 (Northern Italy): A disaster that effective regulation might have prevented. *Nat. Hazards Earth Syst. Sci.* **2012**, *12*, 1029–1044. [[CrossRef](#)]
15. de Oliveira Gomes, L.E.; Correa, L.B.; Sá, F.; Neto, R.R.; Bernardino, A.F. The impacts of the Samarco mine tailing spill on the Rio Doce estuary, Eastern Brazil. *Mar. Pollut. Bull.* **2017**, *120*, 28–36. [[CrossRef](#)]
16. Agurto-Detzel, H.; Bianchi, M.; Assumpção, M.; Schimmel, M.; Collaço, B.; Ciardelli, C.; Barbosa, J.R.; Calhau, J. The tailings dam failure of 5 November 2015 in SE Brazil and its preceding seismic sequence. *Geophys. Res. Lett.* **2016**, *43*, 4929–4936. [[CrossRef](#)]
17. Rotta, L.H.S.; Alcântara, E.; Park, E.; Negri, R.G.; Lin, Y.N.; Bernardo, N.; Mendes, T.S.G.; Souza Filho, C.R. The 2019 Brumadinho tailings dam collapse: Possible cause and impacts of the worst human and environmental disaster in Brazil. *Int. J. Appl. Earth Obs. Geoinf.* **2020**, *90*, 102119.
18. Beauchemin, S.; Langley, S.; MacKinnon, T. Geochemical properties of 40-year old forested pyrrhotite tailings and impact of organic acids on metal cycling. *Appl. Geochem.* **2019**, *110*, 104437. [[CrossRef](#)]
19. Chen, T.; Lei, C.; Yan, B.; Li, L.-l.; Xu, D.-m.; Ying, G.-G. Spatial distribution and environmental implications of heavy metals in typical lead (Pb)-zinc (Zn) mine tailings impoundments in Guangdong Province, South China. *Environ. Sci. Pollut. Res.* **2018**, *25*, 36702–36711. [[CrossRef](#)]
20. Ouyang, J.; Liu, Z.; Zhang, L.; Wang, Y.; Zhou, L. Analysis of influencing factors of heavy metals pollution in farmland-rice system around a uranium tailings dam. *Process Saf. Environ. Prot.* **2020**, *139*, 124–132. [[CrossRef](#)]
21. Dinis, M.d.L.; Fiúza, A.; Futuro, A.; Leite, A.; Martins, D.; Figueiredo, J.; Góis, J.; Vila, M.C. Characterization of a mine legacy site: An approach for environmental management and metals recovery. *Environ. Sci. Pollut. Res.* **2020**, *27*, 10103–10114. [[CrossRef](#)]
22. Hu, W.; Xin, C.; Li, Y.; Zheng, Y.; Van Asch, T.; McSaveney, M. Instrumented flume tests on the failure and fluidization of tailings dams induced by rainfall infiltration. *Eng. Geol.* **2021**, *294*, 106401. [[CrossRef](#)]
23. Mohamed, M.H.; Wilson, L.D.; Headley, J.V.; Peru, K.M. Novel materials for environmental remediation of tailing pond waters containing naphthenic acids. *Process Saf. Environ. Prot.* **2008**, *86*, 237–243. [[CrossRef](#)]
24. Vasile, A.; Milășan, A.R.; Andrei, A.E.; Turcu, R.N.; Drăgoescu, M.F.; Axinte, S.; Mihaly, M. An integrated value chain to iron-containing mine tailings capitalization by a combined process of magnetic separation, microwave digestion and microemulsion-assisted extraction. *Process Saf. Environ. Prot.* **2021**, *154*, 118–130. [[CrossRef](#)]
25. Wang, G.; Tian, S.; Hu, B.; Xu, Z.; Chen, J.; Kong, X. Evolution pattern of tailings flow from dam failure and the buffering effect of debris blocking dams. *Water* **2019**, *11*, 2388. [[CrossRef](#)]
26. Wei, Z.-a.; Yang, Y.-h.; Zhao, H.-j.; Chen, Y.-l. Stability of tailings dam of Xiaodae tailings pond. *J. Northeast. Univ. (Nat. Sci.)* **2016**, *37*, 589.
27. Yu, G.; Song, C.; Pan, Y.; Li, L.; Li, R.; Lu, S. Review of new progress in tailing dam safety in foreign research and current state with development trend in China. *Chin. J. Rock Mech. Eng.* **2014**, *33*, 3238–3248.
28. Gao, H.-Y.; Xu, Z.-M.; Wang, K.; Ren, Z.; Yang, K.; Tang, Y.-J.; Tian, L.; Chen, J.-P. Evaluation of the impact of karst depression-type impoundments on the underlying karst water systems in the Gejiu mining district, southern Yunnan, China. *Bull. Eng. Geol. Environ.* **2019**, *78*, 4673–4688. [[CrossRef](#)]
29. Mackay, I.; Videla, A.; Brito-Parada, P. The link between particle size and froth stability—Implications for reprocessing of flotation tailings. *J. Clean. Prod.* **2020**, *242*, 118436. [[CrossRef](#)]
30. Martín-Moreno, C.; Martín Duque, J.F.; Nicolau Ibarra, J.M.; Muñoz-Martín, A.; Zapico, I. Waste dump erosional landform stability—a critical issue for mountain mining. *Earth Surf. Process. Landf.* **2018**, *43*, 1431–1450. [[CrossRef](#)]
31. Chen, X.; Jing, X.; Chen, Y.; Pan, C.; Wang, W. Tailings dam break: The influence of slurry with different concentrations downstream. *Front. Earth Sci.* **2021**, *9*, 726336. [[CrossRef](#)]

32. Hancock, G. A method for assessing the long-term integrity of tailings dams. *Sci. Total Environ.* **2021**, *779*, 146083. [[CrossRef](#)] [[PubMed](#)]
33. Wei, Z.; Yin, G.; Li, G.; Wang, J.-G.; Wan, L.; Shen, L. Reinforced terraced fields method for fine tailings disposal. *Miner. Eng.* **2009**, *22*, 1053–1059. [[CrossRef](#)]
34. Agapito, L.A.; Bareither, C.A. Application of a one-dimensional large-strain consolidation model to a full-scale tailings storage facility. *Miner. Eng.* **2018**, *119*, 38–48. [[CrossRef](#)]
35. Li, S.; Liang, H.; Li, H.; Ma, J.; Li, B. Minimum Void Ratio Model Established from Tailings and Determination of Optimal Void Ratio. *Geofluids* **2021**, *2021*, 8619121. [[CrossRef](#)]
36. Bi, Q.; Li, C.-h.; Chen, J.-x. Effect of fine particle content on mechanical properties of tailings under high confining pressure. *Arab. J. Geosci.* **2021**, *14*, 942. [[CrossRef](#)]
37. Chen, Q.; Zhang, C.; Yang, C.; Ma, C.; Pan, Z. Effect of fine-grained dipping interlayers on mechanical behavior of tailings using discrete element method. *Eng. Anal. Bound. Elem.* **2019**, *104*, 288–299. [[CrossRef](#)]
38. Li, W.; Coop, M. Mechanical behaviour of Panzhihua iron tailings. *Can. Geotech. J.* **2019**, *56*, 420–435. [[CrossRef](#)]
39. Li, Q.-m.; Yuan, H.-n.; Zhong, M.-h. Safety assessment of waste rock dump built on existing tailings ponds. *J. Cent. S. Univ.* **2015**, *22*, 2707–2718. [[CrossRef](#)]
40. Rico, M.; Benito, G.; Salgueiro, A.; Díez-Herrero, A.; Pereira, H. Reported tailings dam failures: A review of the European incidents in the worldwide context. *J. Hazard. Mater.* **2008**, *152*, 846–852. [[CrossRef](#)]
41. Wang, S.; Mei, G.; Xie, X.; Cui, Y. Analysis on Influence of Tailing Pond Construction on Stability of Surrounding Loose Waste Dump. In Proceedings of the IOP Conference Series: Earth and Environmental Science, Tianjin, China, 24–26 April 2020; p. 012104.
42. Zhang, C.; Chen, Q.; Pan, Z.; Ma, C. Mechanical behavior and particle breakage of tailings under high confining pressure. *Eng. Geol.* **2020**, *265*, 105419. [[CrossRef](#)]
43. Deng, Z.; Wu, S.; Fan, Z.; Yan, Z.; Wu, J. Research on the overtopping-induced breaching mechanism of tailings dam and its numerical simulation. *Adv. Civ. Eng.* **2019**, *2019*, 3264342. [[CrossRef](#)]
44. Gui, R.; He, G. The Effects of Internal Erosion on the Physical and Mechanical Properties of Tailings under Heavy Rainfall Infiltration. *Appl. Sci.* **2021**, *11*, 9496. [[CrossRef](#)]
45. Naeini, M.; Akhtarpoor, A. Numerical analysis of seismic stability of a high centerline tailings dam. *Soil Dyn. Earthq. Eng.* **2018**, *107*, 179–194. [[CrossRef](#)]
46. Liu, Y.; Zhao, X.; Wu, S. Analysis of Static Liquefaction and Numerical Simulation for tailings pond under high depositing rates. *Chin. J. Rock Mech. Eng.* **2014**, *33*, 1158–1168.
47. Marsooli, R.; Wu, W. 3-D finite-volume model of dam-break flow over uneven beds based on VOF method. *Adv. Water Resour.* **2014**, *70*, 104–117. [[CrossRef](#)]
48. Mao, C. *Computational Analysis and Control of Seepage Flow*; China Water Conservancy and Hydropower Publishing House: Beijing, China, 2002.
49. Lu, R.-L.; Sun, D.-P.; Wei, W.; Zhou, J.-j. Numerical simulation of seepage field in the tailing dam with draining seepage system. In Proceedings of the 2013 Fourth International Conference on Digital Manufacturing & Automation, Shinan, China, 29–30 June 2013; pp. 858–861.
50. Junrui, C.; Yanqing, W. Research on multiple-level fracture network model for coupled seepage and stress fields in rock mass. *Chin. J. Rock Mech. Eng.* **2000**, *19*, 712–717.
51. Özer, A.T.; Bromwell, L.G. Stability assessment of an earth dam on silt/clay tailings foundation: A case study. *Eng. Geol.* **2012**, *151*, 89–99. [[CrossRef](#)]
52. Tang, G.-p.; Zhao, L.-h.; Li, L.; Yang, F. Stability charts of slopes under typical conditions developed by upper bound limit analysis. *Comput. Geotech.* **2015**, *65*, 233–240. [[CrossRef](#)]

Disclaimer/Publisher’s Note: The statements, opinions and data contained in all publications are solely those of the individual author(s) and contributor(s) and not of MDPI and/or the editor(s). MDPI and/or the editor(s) disclaim responsibility for any injury to people or property resulting from any ideas, methods, instructions or products referred to in the content.